



## CENTRE DE RECERCA MATEMÀTICA

Title: *How cortical waves drive fission of motile cells*  
Journal Information: *Proceedings of the National Academy of Sciences of the United States of America,*  
Author(s): Flemming S., Font F., Alonso S., Beta C..  
Volume, pages: 117 9, DOI:[10.1073/pnas.1912428117]



# How cortical waves drive fission of motile cells

Sven Flemming<sup>a</sup>, Francesc Font<sup>b,c</sup>, Sergio Alonso<sup>b</sup>, and Carsten Beta<sup>a,d,1</sup>

<sup>a</sup>Institute of Physics and Astronomy, University of Potsdam, 14476 Potsdam, Germany; <sup>b</sup>Department of Physics, Universitat Politècnica de Catalunya, 08034 Barcelona, Spain; <sup>c</sup>Centre de Recerca Matemàtica, 08193 Bellaterra, Barcelona, Spain; and <sup>d</sup>Max Planck Institute for Dynamics and Self-Organization, 37077 Göttingen, Germany

Edited by Joe Lutkenhaus, University of Kansas Medical Center, Kansas City, KS, and approved February 12, 2020 (received for review July 18, 2019)

**Cytokinesis—the division of a cell into two daughter cells—is a key step in cell growth and proliferation. It typically occurs in synchrony with the cell cycle to ensure that a complete copy of the genetic information is passed on to the next generation of daughter cells. In animal cells, cytokinesis commonly relies on an actomyosin contractile ring that drives equatorial furrowing and separation into the two daughter cells. However, also contractile ring-independent forms of cell division are known that depend on substrate-mediated traction forces. Here, we report evidence of an as yet unknown type of contractile ring-independent cytokinesis that we termed wave-mediated cytofission. It is driven by self-organized cortical actin waves that travel across the ventral membrane of oversized, multinucleated *Dictyostelium discoideum* cells. Upon collision with the cell border, waves may initiate the formation of protrusions that elongate and eventually pinch off to form separate daughter cells. They are composed of a stable elongated wave segment that is enclosed by a cell membrane and moves in a highly persistent fashion. We rationalize our observations based on a noisy excitable reaction–diffusion model in combination with a dynamic phase field to account for the cell shape and demonstrate that daughter cells emerging from wave-mediated cytofission exhibit a well-controlled size.**

cytofission | actin waves | reaction–diffusion systems | *Dictyostelium discoideum* | self-organization

**A**mong the most fundamental functions of living cells is their ability to grow and divide. As part of the cell cycle, cell division is tightly orchestrated with replication of the genetic material and distribution of the cellular content among the two daughter cells. The mechanical forces that are required to complete the division process are generated by complex functional structures, such as the mitotic spindle and the actomyosin contractile ring that are operated in conjunction with cell cycle-dependent signaling pathways (1). However, cells may also undergo a more primitive, contractile ring-independent cytofission that depends on substrate-mediated traction forces and relies on the formation of multiple amoeboid leading edges that tear the cell apart (2, 3). This form of traction-mediated cytofission was first observed in *Dictyostelium discoideum* cells that are deficient in myosin II and form oversized, multinucleate cells in suspension (4–6). Later, it was recognized that traction-mediated cytofission is evolutionarily conserved in human cells, where it serves as a mechanism to maintain genomic integrity after failed cytokinesis (7).

Here we show evidence of a form of contractile ring-independent cytofission, where the division into daughter cells is driven by self-organized cortical actin waves. Similar to traditional traction-mediated cytofission, wave-mediated fission occurs in oversized multinucleate *D. discoideum* cells that we generated by electric-pulse–induced cell fusion (8, 9). The structure and dynamics of actin waves in *D. discoideum* are well investigated (10–13). They move across the substrate-attached membrane of the cell (basal waves) and show hallmarks of an excitable system (14–16). Most previous studies of actin waves in *D. discoideum* were carried out in axenic strains, which have been adapted for growth in liquid suspension and thus accumulated mutations that enable a lifestyle relying on macropinocytosis. In

particular, all axenic strains share deletions in the *axeB* gene encoding a homologue of the human RasGAP Neurofibromin (NF1) that controls the size of macropinocytic cups (17). The loss of NF1 results in increased Ras activity and was identified as a well-defined genetic switch that pushes the systems from a quiescent into a wave-forming regime (18). However, common axenic strains contain additional, so far uncharacterized mutations that are essential for efficient growth in liquid media (17). Given the close connection between actin waves and macropinocytosis, these mutations may additionally impact the wave dynamics in axenic cells. For the present study, we therefore decided to use the nonaxenic *D. discoideum* wild-type strain DdB, a clone of the original wild-type field isolate, which is the progenitor of most axenic laboratory strains used today (19). A single knockout of NF1 in the DdB background induces abundant wave formation and thus provides a well-defined system to study the interactions of cortical actin waves with the cell border in a systematic fashion (18).

Our experiments reveal that upon collision with the cell border, basal actin waves may drive the formation of daughter cells that display an elongated shape and move in a highly persistent fashion. A phase field model for the cell shape in combination with a generic nonlinear reaction–diffusion system that mimics intracellular wave formation recovers this regime of wave-mediated cytofission. It predicts a well-controlled range of sizes of the daughter cells that we confirmed in our experiments.

## Results

### Ras Signaling Intensity Controls Wave Formation in Giant Cells.

To study the impact of actin waves on cell shape dynamics and division, we compared giant cells obtained by fusing DdB

### Significance

Cell division is one of the most fundamental processes of life at the cellular level. Here, we report a form of cell division that is driven by self-organized actin waves and, in contrast to conventional cytokinesis in animal cells, does not require the formation of an actomyosin contractile ring. Daughter cells that emerge from this process of wave-mediated cytofission have a well-controlled size and exhibit the so-called fan-shaped phenotype that is characterized by a stable elongated shape and highly persistent locomotion. In the framework of synthetic biology, this primitive form of cell division may serve as a paradigm of how to implement a self-organized proliferation strategy in artificial cells that are equipped with a minimal actin cortex.

Author contributions: S.F., F.F., S.A., and C.B. designed research; S.F., F.F., and S.A. performed research; S.F., F.F., and S.A. analyzed data; and S.F., F.F., S.A., and C.B. wrote the paper.

The authors declare no competing interest.

This article is a PNAS Direct Submission.

Published under the PNAS license.

<sup>1</sup>To whom correspondence may be addressed. Email: beta@uni-potsdam.de.

This article contains supporting information online at <https://www.pnas.org/lookup/suppl/doi:10.1073/pnas.1912428117/-DCSupplemental>.

First published March 11, 2020.

nonaxenic wild-type cells with giant cells that exhibit increased Ras activity, generated by fusing DdB cells deficient in the RasGAP NF1 (Fig. 1). In the giant DdB wild-type cells, no cortical actin waves were observed, similar to earlier recordings of normal-sized DdB cells (18). Actin foci and occasional bursts of short-lived actin patches dominated the dynamics at the bottom membrane (Fig. 1A and Movie S1). Eventually, these cells form multiple amoeboid leading edges that move

apart and induce the well-known process of traction-mediated cytofission (2, 4, 5), resulting in amoeboid daughter cells (SI Appendix, Fig. S1).

In contrast, giant cells with increased Ras activity, obtained by fusing DdB NF1 knockout (KO) cells, displayed abundant wave patterns, as expected from previous results in normal-sized cells (18). These waves showed similar properties to those observed before in giant cells that were obtained by fusing axenic

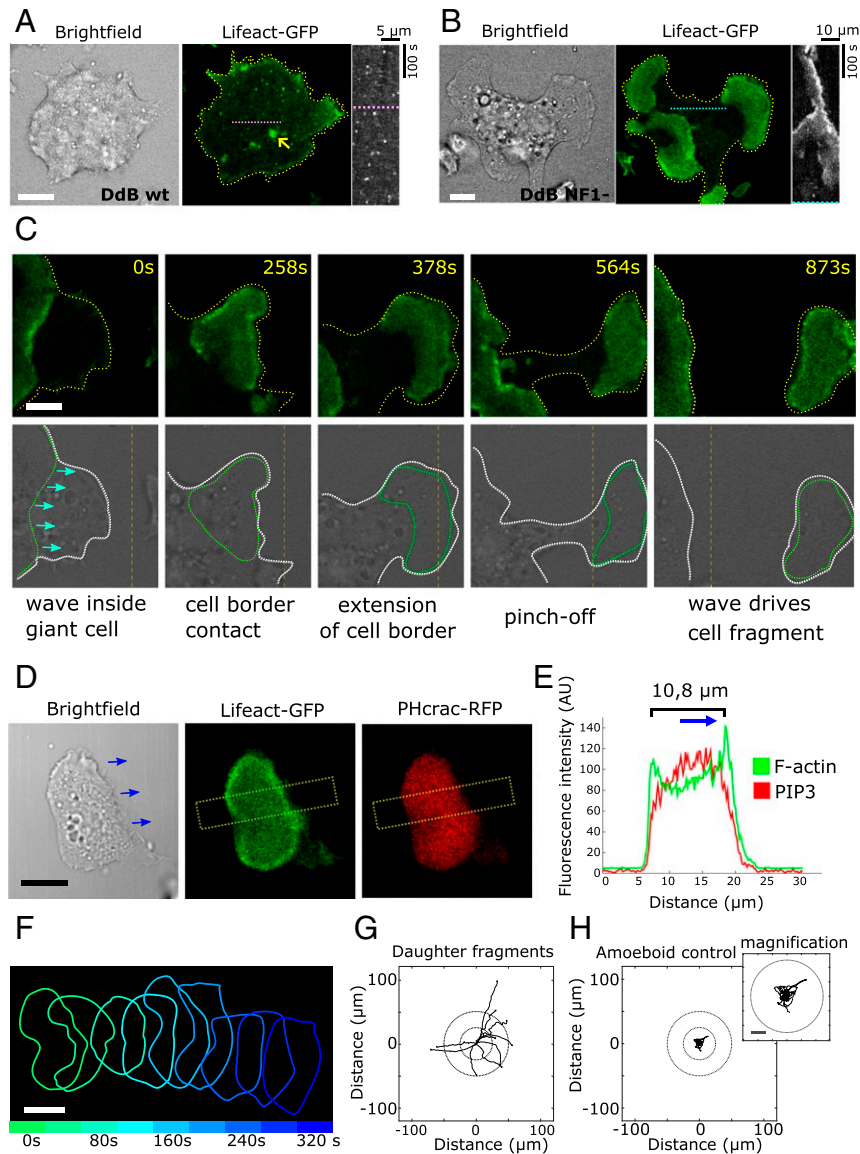


**Fig. 1.** Wave-mediated cytofission. (A) Electrofused DdB wild-type (WT) cell expressing Lifact-GFP. Only F-actin foci and occasional transient F-actin patches (indicated by a yellow arrow) occurred at the surface attached cortex. (Right) A kymograph of the Lifact-GFP signal is shown, displaying the time evolution for 500 s (1 s between frames) along the magenta line shown in the Lifact-GFP image. (B) Electrofused DdB NF1 KO cell expressing Lifact-GFP. Several traveling actin waves are present in this cell. (Right) A kymograph of the Lifact-GFP signal is shown, displaying the time evolution for 500 s (3 s between frames) along the light blue line shown in the Lifact-GFP image. (C) Time series of a wave-mediated fission event. *Top* row shows confocal fluorescence images. *Bottom* row shows the corresponding bright-field images. The shapes of the cell border and of the wave which drives the fission event are depicted by white and green dotted lines, respectively. The field of view in the last frame (873 s) is shifted to the right because the cell moved out of the original frame. As an orientation, a dashed orange line is displayed at a fixed position with respect to the laboratory frame. The direction of wave propagation is indicated by cyan arrows in the first bright-field image. (D) Daughter fragment of a DdB NF1 KO cell expressing Lifact-GFP and PHcrac-RFP, with blue arrows indicating its direction of motion. (E) The profile of the fluorescence intensities along the yellow dotted boxes in D is shown. (F) Outline of the daughter fragment shown in D over 320 s with 40-s intervals. (G and H) Centroid tracks of fan-shaped daughter fragments that emerged from wave-mediated cytofission events (G) and amoeboid control cells (H) (vegetative not fused DdB NF1 KO cells). Each plot shows 10 cell tracks over 10 min with 12 s between time points. The mean speed and directionality of the daughter fragments in G are  $7.1 \pm 1.7 \mu\text{m}/\text{min}$  and  $0.83 \pm 0.09$ , respectively. The mean speed and directionality of the amoeboid cells in H are  $4.0 \pm 1.2 \mu\text{m}/\text{min}$  and  $0.12 \pm 0.06$ , respectively. The cell outline in A–C is indicated by a dashed yellow line. Circles with a radius of 25  $\mu\text{m}$  and 50  $\mu\text{m}$  are shown in G and H. (Scale bars, 10  $\mu\text{m}$ .)

wild-type cells (15) (*SI Appendix, Fig. S2*). They traveled across the substrate-attached bottom membrane and induced strong deformations of the cell–substrate contact area as shown in Fig. 1B and *Movie S2*.

**Basal Actin Waves Drive a Different Type of Cell Fission.** Upon collision with the cell border, basal waves push the membrane outward. In agreement with earlier reports (15), we regularly observed that such collisions led to extinctions of the traveling wave (*SI Appendix, Fig. S2D* and *Movie S2*). However, waves may also drive the formation of more pronounced membrane protrusions that eventually pinch off to form an independent daughter cell, as shown in *Movie S3*.

A detailed view of the individual steps of this process can be seen in Fig. 1C, where a persistently moving wave segment collides with the cell border and pushes the membrane forward. Behind the protruding wave, the connection to the main cell body gradually narrows until a thin cytoplasmic strand is formed that eventually ruptures. In contrast to traditional traction-mediated cytofission, where actin waves are absent and the division process is driven by pseudopod-based motion (ref. 2 and *SI Appendix, Fig. S1*), the traction forces required to complete a wave-mediated cytofission are provided by the propagating actin wave. This becomes obvious when disintegrating the wave by addition of the PI3K inhibitor LY294002 before a wave-mediated cytofission is completed. In *SI Appendix, Fig. S3* two examples are shown, where, upon extinction of the actin wave, a protruding cell front collapses (*SI Appendix, Fig. S3A* and *Movie S4*) and a wave-driven segment that has almost detached from its mother cell reverts to pseudopod-driven motility (*SI Appendix, Fig. S3B* and *Movie S5*). While wave-mediated cytofission is sensitive to PI3K inhibitor treatment, traditional traction-mediated cytofission is not affected. In *SI Appendix, Fig. S4* there are two examples of traction-mediated cytofission after addition of LY294002 to 1) a giant DdB NF1 knockout cell which was in the wave-forming regime (*SI Appendix, Fig. S4A* and *Movie S6*) and 2) a giant DdB wild-type cell (*SI Appendix, Fig. S4B* and *Movie S7*).

The daughter cells that emerge from wave-mediated cytofission consist of the driving wave segment that is now entirely enclosed by the plasma membrane and retains an inner area rich in PIP<sub>3</sub> and F-actin enclosed by a ring of high F-actin concentration (Fig. 1D and E). In giant cells, where enhanced Ras activity due to loss of NF1 results in abundant wave formation, wave-driven divisions are the dominant route of cytofission that leads to complete disintegration of the giant mother cell within a few hours.

**Daughter Cells Originating from Wave-Mediated Fission Are Fan Shaped.** In contrast to the amoeboid daughter cells that result from traction-mediated cytofission of giant wild-type cells, the fragments that are born in a wave-mediated fission event maintain a stable elongated shape and move in a highly persistent manner (Fig. 1F and G). At their leading edge, they frequently show localized protrusions; see *SI Appendix, Fig. S5A* and *B* and *Movie S3* for an example. However, our data suggest that the wave segment that covers most of the substrate-attached membrane is driving the motility of these cells, as the protrusions are usually overrun by the propagating wave or retract without contributing to the movement. This is in accordance with earlier findings which showed that chemotaxis-induced protrusions can be overridden by actin waves (20).

Furthermore, annihilation of the wave by treatment with the PI3K inhibitor LY294002 instantaneously reverts motility of the fragments to the amoeboid type (*SI Appendix, Fig. S5C* and *Movie S8*), similar to the inhibitor treatment of incomplete fission events described above (*SI Appendix, Fig. S3B* and *Movie S5*). Also, the speed of propagation of the daughter cells ( $7.3 \pm$

$1.9 \mu\text{m}/\text{min}$ ) is comparable to the speed of basal waves in the inner part of oversized giant cells before collision with the cell border ( $5.8 \pm 2.0 \mu\text{m}/\text{min}$ ) (*SI Appendix, Fig. S6A*). Overall, the wave-driven daughter cells closely resemble cells that have previously been termed “fan shaped” and were observed as a consequence of the knockout of *amiB* (a gene with a function in aggregation under starvation), under conditions of artificially induced low PIP<sub>2</sub> or high RasC or Rap1 activity levels, and recently also in axenic wild-type strains, when developed at very low cell densities (21–23). Note that a switch from the common amoeboid phenotype (Fig. 1H) to the fan-shaped phenotype is also observed in single DdB NF1 KO cells in the course of development without prior fusion; for more details see also *SI Appendix, SI Materials and Methods*. These fan-shaped cells move at a comparable speed and with similar persistence to the fragments emerging from wave-mediated cytofission (*SI Appendix, Fig. S6*).

**A Generic Reaction–Diffusion Model Recovers the Regime of Cortical Wave Formation.** To rationalize our experimental findings, we introduced a mathematical model that allowed us to explore the interplay of intracellular waves and cell shape dynamics in a systematic fashion. Instead of a detailed mechanistic model, we concentrated on a generic wave-forming reaction–diffusion system for the intracellular dynamics.

The structure of the model is schematically illustrated in Fig. 2A. Intracellular waves are generated by noisy bistable/excitable kinetics with additional mass control to account for intracellular regulation of the amount of  $u$  around a constant level. Typical cell front markers, such as active Ras, PIP<sub>3</sub>, and Arp2/3 that are localized in the inner part of basal actin waves, are represented by elevated values of a lumped activator variable  $u$ . Conversely, regions in the nonexcited, resting state that are characterized by markers of the cell back, such as PIP<sub>2</sub>, myosin II, and cortaxillin, correspond to low values of  $u$ . For a detailed presentation of the model equations, see *SI Appendix*.

Key parameters of the model are the maximal activator level  $u_0$  reached during an excitation (wave amplitude), the parameter  $p$  that sets the intracellular area fraction covered by waves, and the parameter  $b$  that couples the evolution of activator and inhibitor concentrations. It allows for a tuning between different dynamical regimes of the model. The parameter  $a(u)$  dynamically changes the unstable fixed point of the activator–inhibitor system (see the nullclines in Fig. 2B), thereby controlling the threshold for excitations. Fig. 2C–E and *Movies S9–S11* show numerical simulations in a fixed, circular domain that differ only in the values of the parameters  $u_0$  and  $b$ . For low values of  $u_0$  (0.5) only short-lived, spatially restricted patches of the activator are generated (Fig. 2C and *Movie S9*), corresponding to our experimental observations in giant DdB wild-type cells, where the formation of waves is suppressed by high levels of the RasGAP NF1 (Fig. 1A).

In contrast, for high values of  $u_0$  (1.0) propagating waves are generated that display different dynamics, depending on the choice of the coupling parameter  $b$ . If  $b$  is small (0.05), the system displays bistable behavior, where activated regions of high  $u$  concentration form meandering patches that split and coalesce (Fig. 2D and *Movie S10*). With growing values of  $b$  (0.2), the dynamics are shifted toward an excitable regime. Here, regions of increased  $u$  eventually form traveling waves that mutually annihilate upon collision and may even display rotating spiral cores (Fig. 2E and *Movie S11*). This corresponds to the wave dynamics observed in experiments with NF1 knockout cells, where variability between different recordings ranges from bistable to excitable features. Excitable wave dynamics have been extensively analyzed in giant *D. discoideum* cells before (15, 16,

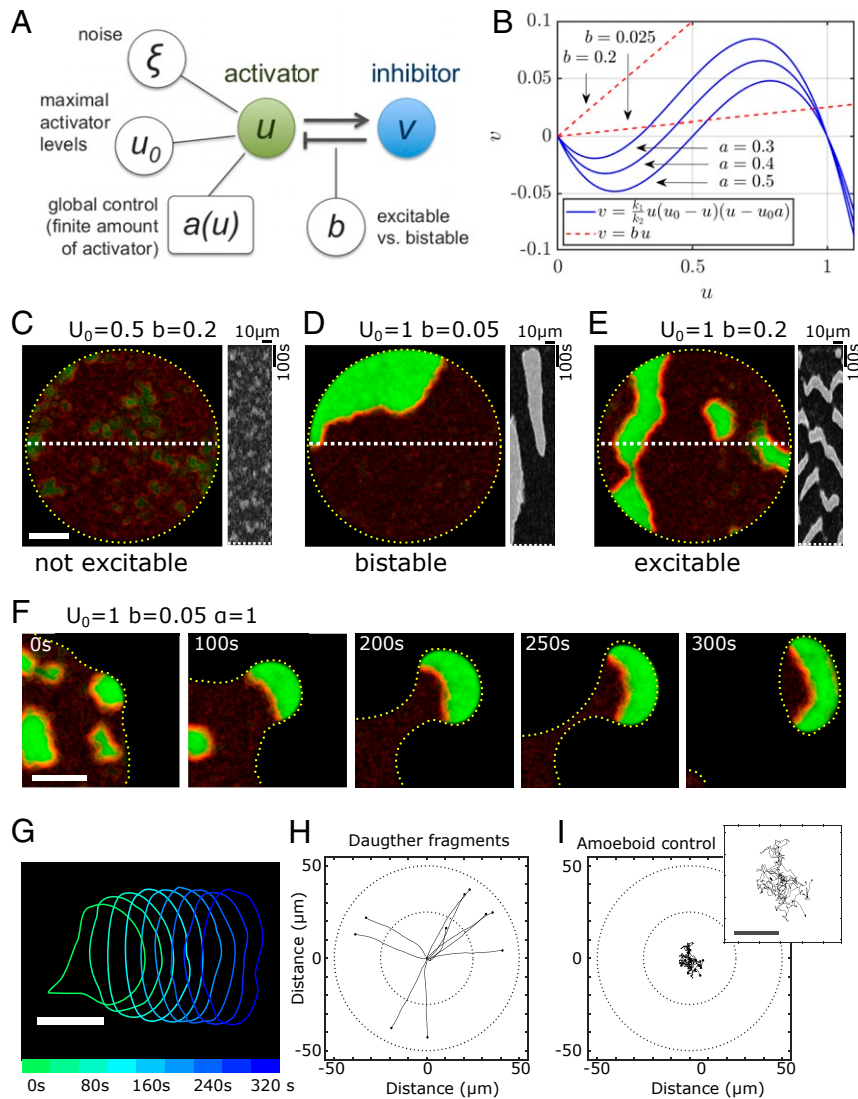


**Fig. 2.** Simulations of wave dynamics in giant cells. (A) Schematic representation of a generic activator–inhibitor model of wave dynamics. The activator concentration  $u$  is influenced by stochastic noise ( $\xi$ ) and the maximal local levels of  $u$  are set by  $u_0$ . Coupling of  $u$  to the inhibitor  $v$  is controlled by the parameter  $b$ , which allows us to tune the system dynamics from a predominantly excitable to a bistable regime. A global constraint defining the total amount of  $u$  is implemented by a dynamically changing  $u$ -dependent parameter  $a$  (Eq. 4). (B) Nullclines of the activator–inhibitor model (Eqs. 1 and 2) for different values of  $a$  and  $b$ . For low total concentrations of  $u$  the dynamic change in  $a$  shifts the nullclines, so that small fluctuations trigger increased wave activity. Decreasing  $b$  decouples the activator  $u$  from the inhibitor  $v$ , which drives the system into a bistable regime. (C–E) Snapshots of simulations for different parameter values of  $u_0$  and  $b$  as indicated above the images. The signal intensity of the green channel is proportional to the concentration of  $u$ . In the red channel, the steepness of the local gradient of  $u$  is displayed to visualize the noise. In all cases, the last time points of simulations with fixed, circular boundaries are shown. In C–E, Right, a kymograph is displayed, taken along the white, dashed line in the respective image (Left) (Movies S9–S11, respectively). (F) Time series of a simulation with the same parameter values as in D, but with dynamically changing boundaries, showing wave-mediated cytofission. (G) Outline of the resulting daughter fragment over 320 s. (H) Centroid tracks of simulated fan-shaped fragments after cytofission from a giant cell with  $u_0 = 1$ ,  $b = 0.05$ , and  $p = 0.25$ . (I) Centroid tracks of simulated amoeboid single cells for comparison (for the choice of parameters, see SI Appendix, Cell Morphodynamics and Pinch-Off). Each plot shows 10 tracks of simulated cells over 10 min with 12 s between time points. The mean speed and directionality of the daughter fragments in H are  $4.0 \pm 0.6 \mu\text{m}/\text{min}$  and  $0.97 \pm 0.05$ , respectively. The mean speed and directionality of the amoeboid cells in I are  $3.6 \pm 0.2 \mu\text{m}/\text{min}$  and  $0.18 \pm 0.06$ , respectively. The outline of the cells in C–F is indicated by a dashed yellow line. Circles with a radius of 25  $\mu\text{m}$  and 50  $\mu\text{m}$  are shown in H and I. (Scale bars, 10  $\mu\text{m}$ .)

20, 24, 25). In the following, we focus on the less-studied bistable regime.

**In Combination with a Dynamical Phase Field to Model the Cell Shape, a Regime of Wave-Mediated Cytofission Is Recovered.** To account for the changing cell shape, we rely on a dynamical phase field that is coupled to the reaction–diffusion system following the method developed by Shao et al. (26). Deformations of the cell shape are driven by an active stress  $\alpha$  that repre-

sents the protrusive forces of the actin cytoskeleton. It pushes the cell boundary outward, depending on the local activator concentration  $u$ . Together with the restoring forces that result from surface tension and volume conservation, these active deformations drive the overall dynamics of the cell shape; see Eqs. 1–4 in Materials and Methods and SI Appendix for the detailed phase field equations.

Upon collision of a wave with the cell border, a protrusion is formed. In the excitable regime (high values of  $b = 0.2$ ),

protruding waves are eventually extinguished by their trailing refractory zone and the membrane relaxes back (Movies S12 and S13) (with  $p = 0.25$  and  $p = 0.5$ , respectively). However, in the bistable regime (low values of  $b = 0.05$ ), activated regions persistently drive the membrane forward and may induce pinch-off of a small daughter cell (Movie S14). The different stages of this fission process are illustrated in Fig. 2F. Except for the long cytoplasmic strands that form under experimental conditions, the cytofission process in the model closely recovers the experimental observations. In particular, the resulting daughter cells consist of a single membrane-enclosed wave segment. With their persistent motion and their stable elongated shape they closely resemble the fan-shaped cells observed in the experiments (Fig. 2 G–I).

**Daughter Cells Originating from Wave-Mediated Cytofission Exhibit a Well-Controlled Size.** A closer analysis of the wave-driven division process revealed several characteristic features that frequently occurred, when basal waves collided with the cell border. We repeatedly observed how broad wave fronts that pushed the membrane forward became unstable and broke up into several smaller wave fragments; see Fig. 3A and Movie S15 for an example. While the smaller fragments shrank and eventually disappeared, the larger ones continued to push the membrane forward and often initiated cytofission events. A similar breakup scenario was found in the bistable regime of our model (Fig. 3B and Movie S16). These observations suggest that only wave segments of a characteristic intermediate size will drive successful cytofission events, so that the daughter fragments will fall into a well-controlled range of sizes. Wave segments that are too small will shrink and die, while large segments will undergo further breakup upon collision with the cell border. We have performed systematic simulations to determine how the wave width and an eventual breakup depend on the model parameters  $b$  and  $p$ , demonstrating that the width of waves decreases with increasing  $b$  and with decreasing  $p$  while breakup occurs toward lower values of  $b$ , depending on the lateral extend of the wave front; see SI Appendix, Fig. S7 for details.

To substantiate the mechanism that leads to a lower size limit of the daughter fragments, we measured, in both experiments and simulations, the maximal area of waves that pushed the cell border forward but did not succeed to initiate cytofission and eventually died; see Fig. 3 C and D for examples. We compared these to the sizes of daughter cells that resulted from successful wave-mediated cytofission events; see Fig. 3 E and F for the corresponding size distributions that were determined from the final fragments that did not divide any further. Even though the sizes of daughter fragments spread over a wider range, the experimental distribution (Fig. 3E) clearly shows a lower size limit corresponding to the size of fan-shaped control cells that emerge when single DdB NF1 KO cells are subject to starvation-induced development.\* By comparison, waves that do not succeed to initiate cytofission display sizes that are, on average, significantly smaller than the smallest daughter fragments, confirming that a minimum wave size is required for wave-driven cytofission. Similarly, also the distributions from numerical simulations in the bistable regime of our model exhibit a clear separation of sizes for successful and unsuccessful cytofission events (Fig. 3F). We furthermore explored how variations in the parameters  $b$  and  $p$  affect the fragment size in our model. With increasing value of  $b$ , we found that the average fragment size as well as the scatter in the range of fragment sizes increases, while the ini-

tial value of  $p$  does not have a strong influence (Fig. 3F and SI Appendix, Fig. S8).

**Wave-Mediated Binary Cytofission.** To explore the consequences of size control of the daughter cells, we systematically changed the size of the mother cell in our numerical simulations. Cells with a size between one and two times the size of a single cell mostly displayed a single stable wave segment. Occasional splittings of the wave resulted in more complex shape deformations but typically, only one of the waves survived, so that no cytofission was observed (Fig. 4A). With increasing cell size, the breakup of waves occurred more regularly and often resulted in the formation of two stable wave fragments, which could tear the cell apart into two daughter cells of similar size (Fig. 4B). The probability of such a binary wave-mediated fission increased with cell size and reached a success rate of almost 100% within a simulation time of 16 min for cells with a size of five times the size of a single cell (Fig. 4A). This finding was confirmed by simulating a growing artificial cell. Once the cellular area exceeded a critical size of four to five times the size of a single cell, wave-mediated cytofission repeatedly occurred, so that on average a constant cell size was maintained; see Fig. 4C and Movie S17 for an example and Fig. 4G for a schematic illustration of wave-mediated binary cytofission in a growing cell.

Similar binary divisions were also observed in experiments with mother cells that emerged from fusing only a few (two to five) DdB NF1 KO cells; see Fig. 4E for an example. The probability to observe a cytofission event within an observation time of 16 min in the experiments increases with the cell size, similar to the model prediction (Fig. 4D). Based on a cell line that expresses a fluorescently tagged histone H2B as a marker of the cell nucleus, we also followed the distribution of nuclei among the daughter cells during wave-mediated cytofission and observed that each fragment contained at least one nucleus (Fig. 4 E and F and SI Appendix, Fig. S9).

## Discussion

Cell cycle-independent cell fission, mediated by cell–substrate traction forces, is a well-known process, which was described for the first time in fish keratocytes, where forces generated in the lamellipodium lead to pinch-off of cell fragments (27). Also oversized *D. discoideum* cells may undergo cell cycle-independent cytofission by forming multiple amoeboid leading edges that move in opposing directions and tear the cell apart in a process that was termed traction-mediated cytofission (2). Later, a similar form of cytofission was also observed in mammalian cells (7).

In this article, we report an as yet unknown variant of cell cycle-independent cytofission, where the division process is driven by self-organized cortical actin waves. This division scenario that we termed wave-mediated cytofission is clearly distinct from the traditional form of traction-mediated cytofission in *D. discoideum*. While both traction-mediated and wave-mediated cytofissions rely on traction forces between the cell and the substrate, the cytoskeletal structures that control and drive the fragmentation process are different. In the case of traditional traction-mediated cytofission, fragmentation is driven by localized pseudopodia that move in different directions and eventually pull the cell apart. In contrast, in the case of wave-mediated cytofission, cortical actin waves that travel across the substrate-attached bottom membrane collide with the cell border and push the membrane forward to form protrusions that eventually separate from the mother cell. To further substantiate that the two fission scenarios rely on different mechanisms, we demonstrated that wave-mediated cytofission, in contrast to traction-mediated cytofission, is sensitive to inhibition of PI3 kinases. Upon treatment with the PI3K inhibitor LY294002, cortical waves are suppressed and wave-mediated cytofission is no longer observed, whereas the traditional form of traction-mediated

\*Note that for the single, not fused control cells, the fan-shaped phenotype displays a larger cross-sectional area compared to the amoeboid phenotype (Fig. 3E) because fan-shaped cells are typically flatter and more spread out on the substrate. This 3D effect is not incorporated into our model, which is intrinsically 2D.

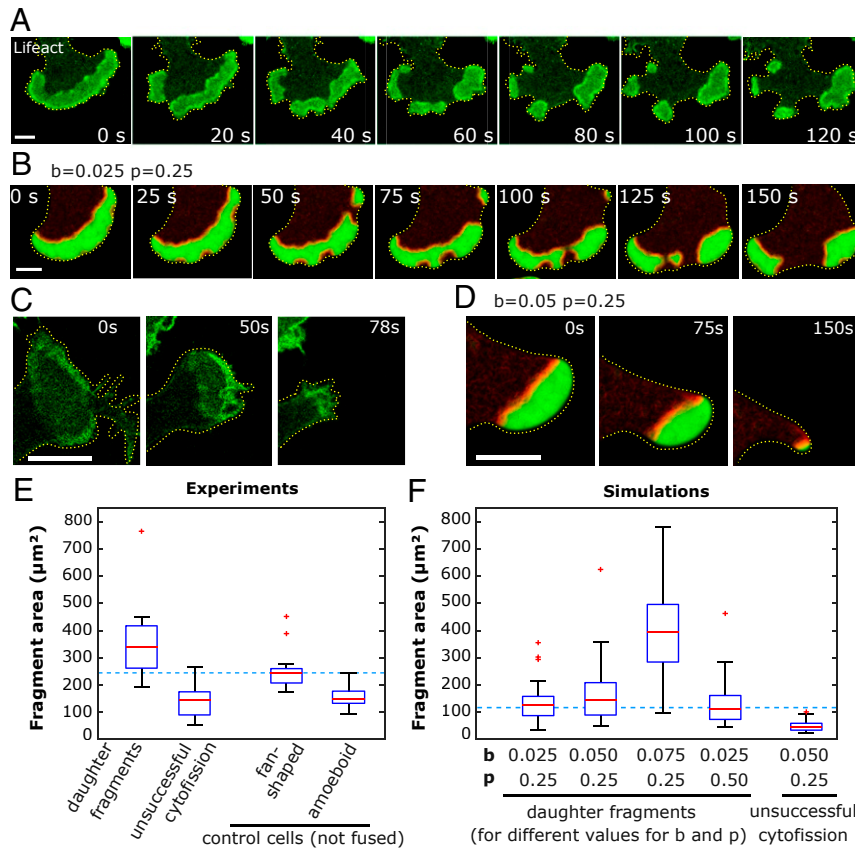


**Fig. 3.** (A and B) Instability of a wave front colliding with the cell border (A) in experiments with giant DdB NF1 KO cells expressing Lifeact-GFP and (B) in numerical simulations ( $\alpha = 1$ ,  $b = 0.025$ ,  $p = 0.25$ ,  $u_0 = 1$ ). (C and D) Unsuccessful wave-mediated cytofission (C) in a giant DdB NF1 KO cell expressing Lifeact-GFP and (D) in numerical simulations ( $b = 0.05$ ,  $p = 0.25$ ). (E) Distribution of final sizes of daughter fragments from wave-mediated cytofission events (21 cells) compared to the maximal size of actin waves that did not lead to successful fission events (20 cells). As a control, we also show the size distributions of single fan-shaped DdB NF1 KO cells (starvation developed, 20 cells) and amoeboid DdB NF1 KO cells (vegetative, 20 cells) that were not fused before (median of the fan-shaped cells marked as dashed blue line). (F) Distribution of final sizes of daughter fragments in simulations with different values for parameters  $b$  and  $p$  as indicated below each box plot. For the parameter setting of  $b = 0.050$  and  $p = 0.25$ , also the maximal sizes of waves that did not lead to a successful fission were measured. For comparison, a reference cell size, given by a disc of  $12 \mu\text{m}$  in diameter (corresponding to a cross-sectional area of  $113 \mu\text{m}^2$ ), is indicated by a dashed blue line. (Scale bars,  $10 \mu\text{m}$ .)

fission remains unaffected. This is in accordance with earlier studies, which showed that PIP3 is dispensable for pseudopod-based amoeboid motility, and clearly distinguishes both forms of cytofission on the biochemical level (28, 29).

Moreover, the daughter cells that are born in a wave-mediated cytofission event exhibit the characteristic fan-shaped phenotype, as opposed to the amoeboid cells that emerge from traditional traction-mediated fission. We observed this division scenario in oversized *D. discoideum* cells that were generated by electric-pulse-induced fusion. The nonaxenic DdB wild-type background used here offers a particularly well-suited framework to study the impact of actin waves on cell-shape dynamics because a single knockout in the *axeB* gene that encodes the RasGAP NF1 induces abundant formation of waves that are absent in the wild type (18). Recently, electro-fused axenic cells (AX2 background) that are also deficient in NF1 were used to study how cortical waves organize the formation of membrane protrusions. In particular, it was found that different protrusive structures, such as pseudopodia, filopodia, or membrane ruffles, are controlled by common regulatory networks (16). Similarly, actin waves are involved in the directional guidance of *D. discoideum* cells across nanostructured surfaces (30). Here, we have demonstrated that the same cortical wave patterns can also drive cytofission into two daughter cells. Previously, it was shown that self-organized excitable wave patterns of Rho signaling and actin assembly play

a role in cell cycle regulation of animal cells (31). Also oscillations in the Min system of *Escherichia coli*, that ensure accurate positioning of the division plane at the center of the rod-shaped cell body (32), rely on a wave-forming dynamical system that could even be reconstituted in vitro (33). However, in these cases self-organized waves assist in the regulation of conventional contractile ring-dependent cytokinesis, whereas in the case of wave-mediated cytofission reported here, actin waves are the key cytoskeletal structures that mechanically drive the division process in the absence of a contractile ring.

We could successfully reproduce the main phenomenological features of wave-mediated cytofission based on a noisy excitable reaction-diffusion system embedded in a dynamic phase field. An additional mass control term was included, to take into account that wave dynamics are affected by the constraints of an enclosed system (34). Our theoretical approach was inspired by a recently introduced model (35), which was developed to describe variability in a population of motile amoeboid cells but did not include the dynamics of intracellular waves, similar to other earlier phase field models (36–39). Previous models that focused on intracellular wave patterns in *D. discoideum* relied on a detailed modular approach; for a review see ref. 40 and references therein. Also wave formation in the upstream signaling pathway (41–44) and at the level of actin polymerization (45) has been considered separately. As opposed to these

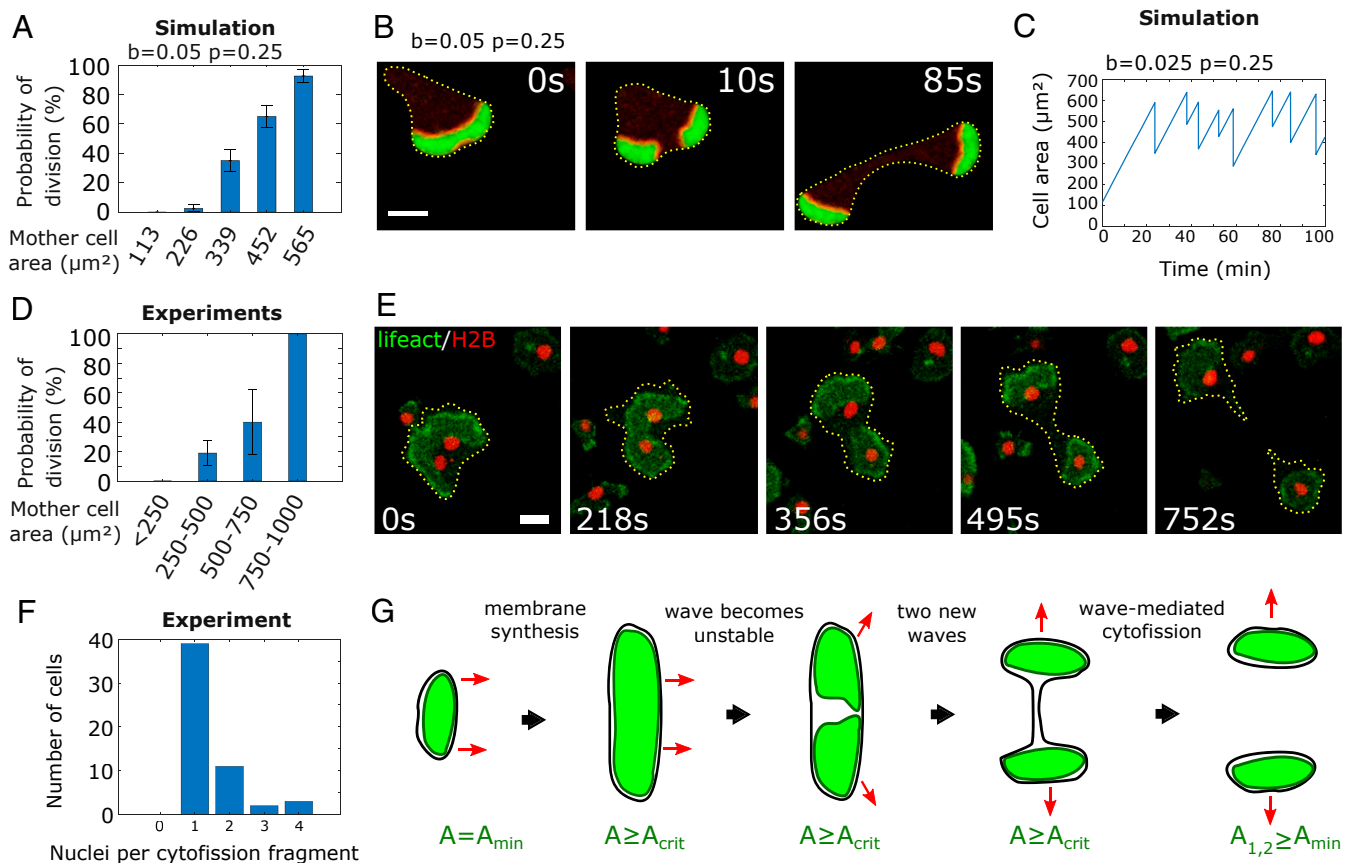


**Fig. 4.** Wave-mediated binary cytofission. (A) Probability of a cytofission event to happen within the first 16 min of a simulation, depending on the cell size. The areas of simulated cells are multiples of a reference cell size of  $113 \mu\text{m}^2$ , given by a disc of  $12 \mu\text{m}$  in diameter. For each cell size 40 independent simulations with  $\alpha = 1$ ,  $b = 0.05$ ,  $p = 0.25$ , and  $u_0 = 1$  were analyzed. Error bars represent the SD and are calculated assuming a binomial distribution. (B) Simulation of a cell with an area of  $339 \mu\text{m}^2$  and the same parameter values used in A. The wave splits into two parts and leads to cytofission. (C) Size evolution of a growing cell over time in a numerical simulation (corresponding to [Movie S17](#)). Once a critical size of about four to five times the size of a single cell is reached, the cell divides via wave-mediated fission into 2 cells of at least the size of a single cell. The graph shows only the size of the larger daughter cells over eight generations. (D) Analysis of the probability of wave-mediated cytofission within the first 16 min of observation for fused DdB NF1 KO cells of different sizes. Cells were categorized according to their area into four groups:  $<250 \mu\text{m}^2$  (10 cells),  $250$  to  $500 \mu\text{m}^2$  (21 cells),  $500$  to  $750 \mu\text{m}^2$  (5 cells), and  $750$  to  $1,000 \mu\text{m}^2$  (5 cells). (E) The actin wave in a fused DdB NF1 knockout cell with two nuclei expressing Lifeact-GFP and histone H2B-RFP becomes unstable and splits into two independent waves that move in opposite directions and induce cytofission. (F) Histogram of the number of nuclei in 55 cytofission fragments obtained from live cell imaging experiments with DdB NF1 knockout cells expressing Lifeact-GFP and histone H2B-RFP. (G) Schematic of wave-mediated binary cytofission in a growing cell.  $A_{\min}$  is the minimal cell area and  $A_{\text{crit}}$  the critical cell size where wave-mediated cytofission starts to occur. (Scale bars,  $10 \mu\text{m}$ .)

more detailed descriptions, our model does not aim at elucidating specific molecular mechanisms. Instead, we designed a reduced model, based on a generic nonlinear wave generator, that highlights the minimal degree of complexity required to describe how cortical waves drive the fission of adherent cells. Our model captures all our observations very well, including the fan-shaped phenotype of the daughter cells, their characteristic range of sizes, the lateral instability of waves that collide with the cell border, and unsuccessful fissions for wave segments below a critical size. Moreover, our analysis demonstrates that wave dynamics need to be appropriately balanced between bistable and excitable regimes (reflected in the choice of model parameter  $b$ ) to reproduce the pinch-off behavior observed in our experiments. Note that bistability was also identified as a key element in describing the dynamics of circular dorsal ruffles, actin-based ring-shaped precursors of macropinocytic cups (46). We believe that a phenomenological modeling approach that identifies the minimal dynamical features needed to recover the experimental observations will be particularly beneficial for guiding future efforts to reconstitute primitive cytofission scenarios in synthetic systems.

The daughter cells that emerged from wave-mediated fission resembled fan-shaped cells that were first observed in knockout cells deficient in the aggregation-related *amiB* gene (21). Recently, it was shown that increased RasC or Rap1 activity, as well as development at very low cell densities, can also induce a switch to the fan-shaped phenotype (22, 23). After wave-mediated cytofission, the ventral membrane of the emerging fan-shaped cell is entirely filled with a wave segment that is known to be rich in active Ras (47). This confirms the key role of increased Ras activity for fan-shaped motility. We thus conclude that the fan-shaped phenotype is generally associated with a stable driving wave segment that covers the ventral cell membrane.<sup>†</sup> This is in agreement with earlier conjectures (12) and has also been suggested by recent modeling of transitions between amoeboid and

<sup>†</sup>Due to their elongated shape and their highly persistent motion, these cells have also been described as “keratocyte-like.” However, to avoid confusion with actual keratocyte fragments (27) that show a very different cytoskeletal organization, we use the recently introduced term “fan shaped” to denote this wave-driven motility phenotype (22).



fan-shaped phenotypes (23). In our model, the switch to a fan-shaped cell is encoded in the parameter  $p$  that sets the intracellular area fraction covered by waves. Systematic numerical simulations revealed that, with increasing  $p$ , the transition to a stable fan-shaped cell occurs at values between  $p = 0.5$  and  $0.6$ , depending on the choice of  $b$ ; see *SI Appendix*, Fig. S10 for more details. Upon wave-mediated cytofission, an increased  $p$  value inherently arises for the newly created daughter cell because most of its area is covered by the driving wave segment.

Furthermore, our experiments revealed that daughter cells emerging from wave-mediated cytofission display a well-controlled range of sizes. While the lower size limit is set by the minimal wave size required to drive a cytofission event, an upper limit is enforced by the breakup of larger waves upon collision with the cell border. Our numerical simulations revealed that the level of excitability, encoded in the model parameter  $b$ , is an important determinant of the fission cell size that increases with growing  $b$ , while the initial value of  $p$  does not have a strong influence (Fig. 3F and *SI Appendix*, Fig. S8). However, the size of the daughter fragments is not determined by the wave width, which decreases with increasing  $b$ , but is rather related to the tendency of waves to break up, which increases for lower  $b$  values (*SI Appendix*, Fig. S7), causing the daughter cells to become smaller on average. In addition, the structural integrity of the microtubule cytoskeleton associated with the individual nuclei is known to influence the nuclear distribution in oversized cells (48) and may thus also affect the sizes of daughter cells in the experiment.

To date, we are not aware of any species where wave-mediated cytofission occurs in the course of native proliferation. However, phylogenetic analyses suggest that the organizing components of the actin cytoskeleton, which are also involved in the formation of actin waves, have already been present in ancestors of eukaryotic cells, where they played an important role in eukaryogenesis (49–51). Thus, similar to traction-mediated cytofission that relies on amoeboid leading edges, we may speculate that wave-mediated cytofission is the remnant of an early form of cell division (52). Our observation that the large majority of fission fragments contain one nucleus supports this hypothesis. We furthermore expect that wave-mediated cytofission is not specific to *D. discoideum* but may occur also in other systems as actin waves are abundantly observed in a wide range of different cell types including neutrophils (53), fish keratocytes (54), fibroblasts (55), and neurons (56, 57); see also refs. 58 and 59 and references therein.

With the advent of synthetic biology, primitive forms of cell division have attracted increasing attention as it remains a major challenge to endow synthetic cellular compartments with the capacity to grow and divide. A primitive form of cell division that relies on emergent actin waves may serve as a promising blueprint of how to implement a self-organized proliferation strategy in artificial vesicles that are equipped with a minimal actin cortex. Here, this was highlighted by our observation that a critical cell size is required to induce wave-mediated cytofission. Consequently, a growing cell maintains a well-defined average

size by undergoing a repeated sequence of wave-mediated fission events (Fig. 4 C and G and *Movie S17*). By tuning between different regimes of wave dynamics, the rate of cell division can be enhanced or decreased. Moreover, the versatile character of actin waves would also allow driving other cellular functions, such as intracellular transport and motility.

## Materials and Methods

**Cell Strains, Culture Conditions, and Cell Fusion.** All experiments were performed with nonaxenic *D. discoideum* strains. DdB wild-type and DdB NF1 KO cells were cultivated in Sørensen's buffer supplemented with *Klebsiella aerogenes*,  $MgCl_2$ , and  $CaCl_2$ . Plasmids for reporter expression were cloned based on plasmids for extrachromosomal expression in nonaxenic strains (60). To create oversized cells, 2- to 3-h starved cells were fused via electric pulses as described before (8, 9, 15). For detailed experimental procedures see *SI Appendix*, *SI Materials and Methods*.

**Mathematical Methods.** The computational model employed for the description of the dynamics of giant *D. discoideum* cells is based on two coupled reaction–diffusion equations,

$$\frac{\partial(\phi u)}{\partial t} = \phi [k_1 u (u_0 - u)(u - u_0 a(u)) - k_2 v + \xi(\mathbf{x}, t)] + \nabla \cdot (\phi D_u \nabla u), \quad [1]$$

$$\frac{\partial(\phi v)}{\partial t} = \phi \varepsilon (b u - v) + \nabla \cdot (\phi D_v \nabla v), \quad [2]$$

where  $\xi$  is an Ornstein–Uhlenbeck noise and  $\phi$  is a phase field which takes the values 1 and 0 inside and outside the cell, respectively. The variable  $u$  is coupled to a dynamical equation for the phase field describing the shape and deformation of the cell:

$$\tau \frac{\partial \phi}{\partial t} = \gamma \left( \nabla^2 \phi - \frac{G'(\phi)}{\varepsilon^2} \right) - \beta \left( \int \phi dx - A_0 \right) |\nabla \phi| + \alpha u |\nabla \phi|. \quad [3]$$

We include into the equations a global control term that accounts for the regulation of the total amount of  $u$  around a constant level,

$$a(u) = a_0 + M \left( \int \frac{u}{u_0} dA - p A_0 \right). \quad [4]$$

The stochastic partial differential equations have been integrated with standard finite differences methods. For more information about the model and specific parameter values see *SI Appendix*.

**Data Availability.** All data are shown in this article or are available in *SI Appendix*. Plasmid constructs and cell lines used in this study are available at <http://www.dictybase.org>. Scripts for image processing used in this work will be provided on demand by the corresponding author.

**ACKNOWLEDGMENTS.** We thank Peggy Paschke and Rob Kay (Medical Research Council [MRC] Laboratory of Molecular Biology, Cambridge, UK) for providing cell lines and technical support. S.F. and C.B. gratefully acknowledge funding by the Deutsche Forschungsgemeinschaft in the framework of Sonderforschungsbereich (SFB) 937, Project A09 and SFB 1294, Project B02. S.A. and F.F. acknowledge support from Ministerio de Ciencia, Innovación y Universidades (MCIU), Agencia Estatal de Investigación (AEI), and Fondo Europeo de Desarrollo Regional (FEDER) under Projects PGC2018-095456-B-I00, FIS2014-55365-P, and RYC-2012-11265. F.F. acknowledges financial support from the Obra Social la Caixa through the program Recerca en Matemàtica Col·laborativa and the Centres de Recerca de Catalunya (CERCA) Program of the Generalitat de Catalunya.

- J. P. Fededa, D. W. Gerlich, Molecular control of animal cell cytokinesis. *Nat. Cell Biol.* **14**, 440–447 (2012).
- T. Q. P. Uyeda, A. Nagasaki, Variations on a theme: The many modes of cytokinesis. *Curr. Opin. Cell Biol.* **16**, 55–60 (2004).
- M. Kanada, A. Nagasaki, T. Q. P. Uyeda, Adhesion-dependent and contractile ring-independent equatorial furrowing during cytokinesis in mammalian cells. *Mol. Biol. Cell* **16**, 3865–3872 (2005).
- D. A. Knecht, W. F. Loomis, Antisense RNA inactivation of myosin heavy chain gene expression in *Dictyostelium discoideum*. *Science* **236**, 1081–1086 (1987).
- A. De Lozanne, J. A. Spudich, Disruption of the *Dictyostelium* myosin heavy chain gene by homologous recombination. *Science* **236**, 1086–1091 (1987).
- R. Neujahr, C. Heizer, G. Gerisch, Myosin II-independent processes in mitotic cells of *Dictyostelium discoideum*: Redistribution of the nuclei, re-arrangement of the actin system and formation of the cleavage furrow. *J. Cell Sci.* **110**, 123–137 (1997).

- A. Choudhary et al., Interphase cytofission maintains genomic integrity of human cells after failed cytokinesis. *Proc. Natl. Acad. Sci. U.S.A.* **110**, 13026–13031 (2013).
- E. Neumann, G. Gerisch, K. Opatz, Cell fusion induced by high electric impulses applied to *Dictyostelium*. *Naturwissenschaften* **67**, 414–415 (1980).
- G. Gerisch et al., Membrane and actin reorganization in electropulse-induced cell fusion. *J. Cell Sci.* **126**, 2069–2078 (2013).
- M. G. Vicker, W. Xiang, P. J. Plath, W. Wosniok, Pseudopodium extension and amoeboid locomotion in *Dictyostelium discoideum*: Possible autowave behaviour of F-actin. *Nonlinear Phenom.* **101**, 317–332 (1997).
- G. Gerisch et al., Mobile actin clusters and traveling waves in cells recovering from actin depolymerization. *Biophys. J.* **87**, 3493–3503 (2004).
- Y. Asano, A. Nagasaki, T. Q. P. Uyeda, Correlated waves of actin filaments and PIP3 in *Dictyostelium* cells. *Cell Motil. Cytoskeleton* **65**, 923–934 (2008).

13. M. Jasnin *et al.*, The architecture of traveling actin waves revealed by cryo-electron tomography. *Structure* **27**, 1211–1223.e5 (2019).
14. T. Bretschneider *et al.*, The three-dimensional dynamics of actin waves, a model of cytoskeletal self-organization. *Biophys. J.* **96**, 2888–2900 (2009).
15. M. Gerhardt *et al.*, Actin and PIP3 waves in giant cells reveal the inherent length scale of an excited state. *J. Cell Sci.* **127**, 4507–4517 (2014).
16. Y. Miao *et al.*, Wave patterns organize cellular protrusions and control cortical dynamics. *Mol. Syst. Biol.* **15**, e8585 (2019).
17. G. Bloomfield *et al.*, Neurofibromin controls macropinocytosis and phagocytosis in *Dictyostelium*. *eLife* **4**, e04940 (2015).
18. D. M. Veltman *et al.*, A plasma membrane template for macropinocytic cups. *eLife* **5**, e20085 (2016).
19. G. Bloomfield, Y. Tanaka, J. Skelton, A. Ivens, R. R. Kay, Widespread duplications in the genomes of laboratory stocks of *Dictyostelium discoideum*. *Genome Biol.* **9**, R75 (2008).
20. M. Ecke, G. Gerisch, Co-existence of Ras activation in a chemotactic signal transduction pathway and in an autonomous wave-forming system. *Small GTPases* **10**, 72–80 (2017).
21. Y. Asano *et al.*, Keratocyte-like locomotion in amiB-null *Dictyostelium* cells. *Cell Motil. Cytoskeleton* **59**, 17–27 (2004).
22. Y. Miao *et al.*, Altering the threshold of an excitable signal transduction network changes cell migratory modes. *Nat. Cell Biol.* **19**, 329–340 (2017).
23. Y. Cao, E. Ghabache, W.-J. Rappel, Plasticity of cell migration resulting from mechanochemical coupling. *eLife* **8**, e48478 (2019).
24. M. Lange, J. Prassler, M. Ecke, A. Müller-Taubenberger, G. Gerisch, Local Ras activation, PTEN pattern, and global actin flow in the chemotactic responses of oversized cells. *J. Cell Sci.* **129**, 3462–3472 (2016).
25. M. Jasnin, M. Ecke, W. Baumeister, G. Gerisch, Actin organization in cells responding to a perforated surface, revealed by live imaging and cryo-electron tomography. *Structure* **24**, 1031–1043 (2016).
26. D. Shao, W.-J. Rappel, H. Levine, Computational model for cell morphodynamics. *Phys. Rev. Lett.* **105**, 108104 (2010).
27. U. Euteneuer, M. Schliwa, Persistent, directional motility of cells and cytoplasmic fragments in the absence of microtubules. *Nature* **310**, 58–61 (1984).
28. O. Hoeller, R. R. Kay, Chemotaxis in the absence of PIP3 gradients. *Curr. Biol.* **17**, 813–817 (2007).
29. K. Takeda, A. T. Sasaki, H. Ha, H.-A. Seung, R. A. Firtel, Role of phosphatidylinositol 3-kinases in chemotaxis in *Dictyostelium*. *J. Biol. Chem.* **282**, 11874–11884 (2007).
30. X. Sun *et al.*, Asymmetric nanotopography biases cytoskeletal dynamics and promotes unidirectional cell guidance. *Proc. Natl. Acad. Sci. U.S.A.* **112**, 12557–12562 (2015).
31. W. M. Bement *et al.*, Activator-inhibitor coupling between Rho signalling and actin assembly makes the cell cortex an excitable medium. *Nat. Cell Biol.* **17**, 1471–1483 (2015).
32. P. A. de Boer, R. E. Crossley, L. I. Rothfield, A division inhibitor and a topological specificity factor coded for by the minicell locus determine proper placement of the division septum in *E. coli*. *Cell* **56**, 641–649 (1989).
33. M. Loose, E. Fischer-Friedrich, J. Ries, K. Kruse, P. Schwill, Spatial regulators for bacterial cell division self-organize into surface waves in vitro. *Science* **320**, 789–792 (2008).
34. D. A. Kessler, H. Levine, Nonlinear self-adapting wave patterns. *New J. Phys.* **18**, 122001 (2016).
35. S. Alonso, M. Stange, C. Beta, Modeling random crawling, membrane deformation and intracellular polarity of motile amoeboid cells. *PLoS One* **13**, e0201977 (2018).
36. D. Shao, H. Levine, W.-J. Rappel, Coupling actin flow, adhesion, and morphology in a computational cell motility model. *Proc. Natl. Acad. Sci. U.S.A.* **109**, 6851–6856 (2012).
37. F. Ziebert, S. Swaminathan, I. S. Aranson, Model for self-polarization and motility of keratocyte fragments. *J. R. Soc. Interface* **9**, 1084–1092 (2012).
38. S. Najem, M. Grant, Phase-field approach to chemotactic driving of neutrophil morphodynamics. *Phys. Rev. E* **88**, 034702 (2013).
39. A. Moure, H. Gomez, Computational model for amoeboid motion: Coupling membrane and cytosol dynamics. *Phys. Rev. E* **94**, 042423 (2016).
40. P. N. Devreotes *et al.*, Excitable signal transduction networks in directed cell migration. *Annu. Rev. Cell Dev. Biol.* **33**, 103–125 (2017).
41. Y. Arai *et al.*, Self-organization of the phosphatidylinositol lipids signaling system for random cell migration. *Proc. Natl. Acad. Sci. U.S.A.* **107**, 12399–12404 (2010).
42. D. Taniguchi *et al.*, Phase geometries of two-dimensional excitable waves govern self-organized morphodynamics of amoeboid cells. *Proc. Natl. Acad. Sci. U.S.A.* **110**, 5016–5021 (2013).
43. M. Hörning, T. Shibata, Three-dimensional cell geometry controls excitable membrane signaling in *Dictyostelium* cells. *Biophys. J.* **116**, 372–382 (2019).
44. S. Fukushima, S. Matsuoka, M. Ueda, Excitable dynamics of Ras triggers spontaneous symmetry breaking of PIP3 signaling in motile cells. *J. Cell Sci.* **132**, jcs224121 (2019).
45. A. Dreher, I. S. Aranson, K. Kruse, Spiral actin-polymerization waves can generate amoeboid cell crawling. *New J. Phys.* **16**, 055007 (2014).
46. E. Bernitt, H.-G. Döbereiner, N. S. Gov, A. Yochelis, Fronts and waves of actin polymerization in a bistability-based mechanism of circular dorsal ruffles. *Nat. Commun.* **8**, 15863 (2017).
47. G. Gerisch, M. Ecke, D. Wischniewski, B. Schroth-Diez, Different modes of state transitions determine pattern in the phosphatidylinositol-Actin system. *BMC Cell Biol.* **12**, 42 (2011).
48. M. Stange *et al.*, Analyzing the spatial positioning of nuclei in polynuclear giant cells. *J. Phys. D Appl. Phys.* **50**, 464001 (2017).
49. N. Yutin, M. Y. Wolf, Y. I. Wolf, E. V. Koonin, The origins of phagocytosis and eukaryogenesis. *Biol. Direct* **4**, 9 (2009).
50. T. Cavalier-Smith, Predation and eukaryote cell origins: A coevolutionary perspective. *Int. J. Biochem. Cell Biol.* **41**, 307–322 (2009).
51. J. B. Dacks *et al.*, The changing view of eukaryogenesis - fossils, cells, lineages and how they all come together. *J. Cell Sci.* **129**, 3695–3703 (2016).
52. T. Q. Uyeda, C. Kitayama, S. Yumura, Myosin II-independent cytokinesis in *Dictyostelium*: Its mechanism and implications. *Cell Struct. Funct.* **25**, 1–10 (2000).
53. O. D. Weiner, W. A. Marganski, L. F. Wu, S. J. Altschuler, M. W. Kirschner, An actin-based wave generator organizes cell motility. *PLoS Biol.* **5**, e221 (2007).
54. E. L. Barnhart, K.-C. Lee, K. Keren, A. Mogilner, J. A. Theriot, An adhesion-dependent switch between mechanisms that determine motile cell shape. *PLoS Biol.* **9**, e1001059 (2011).
55. C. Guetta-Terrier *et al.*, Protrusive waves guide 3d cell migration along nanofibers. *J. Cell Biol.* **211**, 683–701 (2015).
56. M. Toriyama *et al.*, Shootin1: A protein involved in the organization of an asymmetric signal for neuronal polarization. *J. Cell Biol.* **175**, 147–157 (2006).
57. A. M. Winans, S. R. Collins, T. Meyer, Waves of actin and microtubule polymerization drive microtubule-based transport and neurite growth before single axon formation. *eLife* **5**, e12387 (2016).
58. N. Inagaki, H. Katsuno, Actin waves: Origin of cell polarization and migration?. *Trends Cell Biol.* **27**, 515–526 (2017).
59. C. Beta, K. Kruse, Intracellular oscillations and waves. *Annu. Rev. Condens. Matter Phys.* **8**, 239–264 (2017).
60. P. Paschke *et al.*, Rapid and efficient genetic engineering of both wild type and axenic strains of *Dictyostelium discoideum*. *PLoS One* **13**, e0196809 (2018).